Journal of Applied Physics

RESEARCH ARTICLE | JULY 08 2025

Impact of water absorption on electrical properties of epoxy composite polymers: Suppressed charge trapping and enhanced ion transport

Luigi Balestra ; Mattia Rossetti ; Elena Gnani ; Susanna Reggiani

J. Appl. Phys. 138, 025105 (2025)
https://doi.org/10.1063/5.0263738

Journal of Applied Physics ARTICLE pubs.aip.org/aip/jap

Impact of water absorption on electrical properties of epoxy composite polymers: Suppressed charge trapping and enhanced ion transport

Cite as: J. Appl. Phys. **138**, 025105 (2025); doi: 10.1063/5.0263738
Submitted: 6 February 2025 · Accepted: 16 June 2025 ·
Published Online: 8 July 2025

Luigi Balestra,[1,a)] Mattia Rossetti,[2] Elena Gnani,[1] and Susanna Reggiani[1]

AFFILIATIONS

[1]ARCES and DEI, University of Bologna, Bologna, Italy
[2]Smart Power R&D, STMicroelectronics, Cornaredo, Italy

[a)]**Author to whom correspondence should be addressed:** luigi.balestra5@unibo.it

ABSTRACT

Epoxy-based molding compounds (EMCs) are nowadays widely used as encapsulating materials in integrated circuits (ICs) due to their excellent mechanical and electrical properties. Their application to smart power high-voltage ICs is under intensive study as harsh environment conditions exacerbate their performance. More specifically, the presence of a leakage current and the accumulation of space charge under high humidity can affect their long-term reliability, leading to die-level and package-level failures. In this work, by performing transient current measurements and employing numerical simulations, the role of moisture on the EMC properties is investigated. Experiments show that dry samples exhibit the expected current decrease with time before reaching a steady-state regime. Simulations confirm the key role of charge trapping and trap-assisted recombination in the definition of the final leakage current. In contrast, wet samples show unique behavior when subjected to sufficiently high electric fields: the usual reduction of the current is followed by a strong current increase without reaching an equilibrium condition. Simulations reveal that suppressed trapping phenomena allow for a reduction of the net space charge leading to the observed current rise. Moreover, the absence of a steady state and the sharp current increase at large stress times are attributed to enhanced ion transport because of the large presence of water molecules.

I. INTRODUCTION

Epoxy-based composite polymers, due to their excellent mechanical and electrical properties, have found extensive applications in various fields ranging from aerospace and automotive to electronic applications.[1,2] More specifically, an epoxy mold compound (EMC) with a large fraction of silica fillers is nowadays widely used in the electronic industry as encapsulation material for high voltage integrated circuits (HV-ICs). Due to their outstanding properties, they are able to match the thermal expansion coefficient of the silicon die and, at the same time, exhibit a low water absorption coefficient. In general, they can provide protection to the underneath devices even under an extreme environmental condition with high temperature and a large amount of moisture.[3] Nevertheless, the presence of leakage current and the accumulation of space charge inside the EMC can lead to long-term reliability issues due to the distortion of the electrostatic potential with consequent degradation of the HV-IC performance.[4,5] Moreover, the presence of ions can lead to electrochemical corrosion of the bonding wire.[6] Despite the reduced water uptake when compared with other materials, the small amount of water absorbed by the EMC can still lead to significant changes in its material properties. Several studies have shown how humidity can lead to swelling and changes in the glass transition temperature of the material.[7] In addition, significant variations of the EMC electrical properties have been observed under wet conditions. Pulsed electro-acoustic (PEA) measurements on thick EMC samples have shown a reduced amount of homo-charge and the formation of hetero-charge at

large stress time, which can be ascribed to the presence of ions.[8] Mamun *et al.*,[9] by intentionally introducing $MgCl_2$ in wet EMC samples, have demonstrated that in the low field conditions (up to 500 V on a 0.7 mm thick sample), ionic transport provides the dominant contributions to leakage current at low stress times, while it becomes negligible at high stress times due to its dispersive nature. Moreover, this leads to strong formation of a hetero-charge giving rise, under wet conditions, to a leakage current increase due to an enhanced electron injection. In our previous works, an anomalous current increase with time was observed during conductivity measurements performed on wet interdigitated capacitors with 15.7 μm dielectric thickness under large electric fields.[10,11] In this work, new experiments reveal that after an initial decrease of current over time, it subsequently increases depending on the applied voltage biases and humidity conditions. Additionally, at high stress times, a sharp increase is observed, which can be recognized by a significant change in the slope of the curve. These variations suggest the presence of two different underlying physical mechanisms behind the high leakage of wet EMC samples, which cannot be fully explained in terms of hetero-charge formation due to ionic transport. We demonstrate, through an extended characterization of the EMC transient current and a complete simulation approach, that charge trapping effects might be suppressed by the presence of water. Moreover, the absence of a steady-state condition is associated with the formation of a hetero-charge induced by the accumulations of ions close to the electrodes. This is facilitated by significantly large ionic mobility, which is enhanced by the presence of water molecules.

This paper is organized as follows: Sec. II provides a description of the experimental setup and shows the outcomes of the measurements. In Sec. III, the numerical model used to emulate the transient current characteristics is described, and the roles of traps and moisture are explained. Thus, experiments and simulations are compared in Sec. IV. Conclusions are presented in Sec. V. In the Appendix, the differential equations that compose the bipolar charge transport are reported together with the corresponding boundary conditions and full parameter sets.

II. MEASUREMENT SETUP AND EXPERIMENTAL RESULTS

A. Test structure and measurement details

The test structure adopted in this work is an interdigitated capacitor with an exposed area of 10^{-7} m^2 and a dielectric thickness of 15.7 μm. A schematic representation of the structure is reported in Fig. 1. Devices are manufactured close to the center of a 4.2×2.6 mm^2 silicon die. It is the same device adopted in previous analyses,[10,11] with peculiar features relevant to address charge-transport properties specifically correlated to the final application: (i) the proposed structure allows for the application of very large electric fields, closer to the breakdown voltage, due to the limited thickness between the embedded electrodes; (ii) significant absorption of water is reached after 48 h for such limited volumes with diffusion saturation at 24 h and the non-Fickian trends due to a water reaction expected to become relevant for longer exposure times,[12] allowing for interesting experimental investigations; and (iii) the structure allows one to effectively measure electrical conductivity of the material at electric fields comparable with those expected in high-voltage integrated circuits and packaging. The composite polymer under investigation is a commercial biphenyl/multiaromatic resin with a 88 wt. % spherical silica filler. All samples are dried in a thermostatic oven for 48 h at 100 °C in order to remove pre-existing humidity. Some of them are exposed to 85 °C/85%RH for 96 or 168 h in a climatic chamber. A Keithley 2290-5 5 kV power supply and Keysight B2981-A picoammeter are used to generate the step voltage of the DC bias and measure the current as a function of time, $i(t)$, respectively. All measurements are performed at room temperature (T = 300 K). For each bias and precondition, multiple measurements are performed on different samples: the $i(t)$ curves reported in Sec. II B always represent the averaged current measured across the different samples. The experienced variability is not critical and does not influence the extraction of the main observed features.

B. Transient current measurements

In Fig. 2(a), the polarization currents $i(t)$ of dry samples are reported as functions of time after the voltage step for different values of the DC bias V_{DC}. As expected, they show a current decrease with time independently of the applied voltage and then reach a steady-state condition in approximately 10^4 s. In Fig. 2(b), the corresponding steady-state conductivity is reported, calculated as $\sigma = I \cdot d/(V_{DC} \cdot A)$, with I being the current extracted in a steady state, d the nominal thickness of the capacitor, V_{DC} the value of a DC bias, and A the active area of the interdigitated electrodes. A clear exponential field dependence of the conductivity is observed, which can be attributed to either the enhanced charge hopping at higher electric fields or the Schottky-barrier lowering, or a combination of the two. The physical phenomena affecting the current transport of such EMCs in dry conditions are, thus, due to the bulk material and the Schottky-barrier boundary, as previously shown by simulations performed with the Sentaurus Technology Computer Aided Design (TCAD) tool.[10,11] It is worth noting that the presence of a space charge can cause significant field distortion, which may significantly affect the charge injection at electrodes, thus contributing to the observed field dependence of the conductivity.

In Fig. 3, the $i(t)$ measurements in wet samples are reported for two different values of exposure time in the climatic chamber. At a low bias, they behave similarly to the dry ones, showing a current reduction with time up to the steady state. By comparing the $i(t)$ curves of dry and wet samples at low biases, the current decreases with time according to an inverse power law, i.e., $i(t) \propto t^{-s}$. This is typical of disordered polymeric insulators, where hopping between localized states in a structurally and energetically heterogeneous system leads to a broad distribution of relaxation times, resulting in a non-exponential current decay.[13] In contrast, at high voltages, completely different behavior is observed: after an initial decrease with time, the current increases by several orders of magnitude. In addition, instead of reaching a steady-state condition, a sharp increase of current is observed for the higher applied voltage at $t \geq 10^4$ s. As a consequence, it is not possible to extract a value of the DC conductivity in wet conditions at high electric fields. Finally, the role of the amount of moisture uptake in such

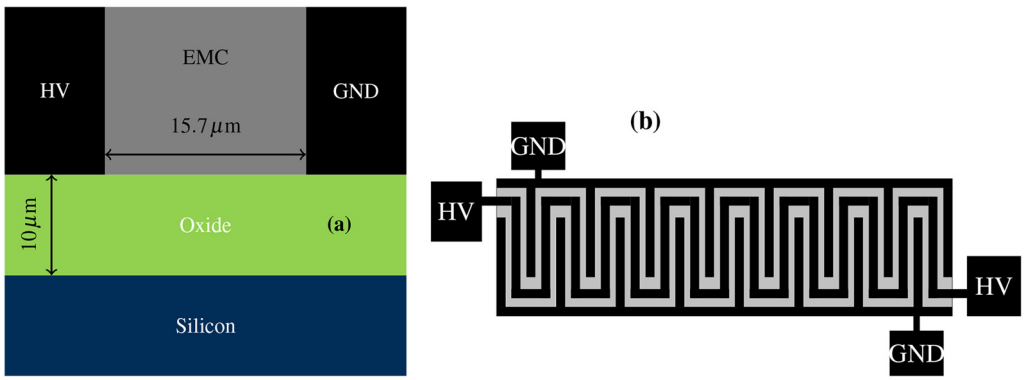

FIG. 1. (a) Cross-sectional schematic of the test structure. The capacitor is manufactured above a silicon die with a 10 μm layer of SiO_2 on top. (b) Top view showing the interdigitated structure of the fabricated device. The proposed snake-comb capacitor is realized enclosed in a power shrink small outline (SSO) package.

kind of EMCs is further analyzed. Significant absorption of water is reached after 48 h by moisture diffusion,[12] while the non-Fickian trend due to a water reaction is expected to cause an additional moisture income with longer exposure times. For this reason, a relevant increase of the leakage current and a slight anticipation of the sharp slope rise are observed at large electric fields for the data with a preconditioning of 168 h with respect to the case of 96 h. The experimental data uncover the sharp increase at larger stress times, which was only partially addressed in the previous analyses.[10,11] The previously proposed TCAD outcomes were focused mostly on the anomalous current increase with clear deficiencies in the prediction of the different slopes of the $i(t)$ curves. So far, the in-depth understanding of the current characteristics in wet conditions is missing, and the TCAD simulations proposed in the previous works suffer for the limited set of equations. A different simulation approach is required to accurately model the physical phenomena related to injected electron/hole charges, trapped charges in the EMC bulk, and, eventually, ionic transport under wet conditions. The modeling issue is fully addressed in Sec. III.

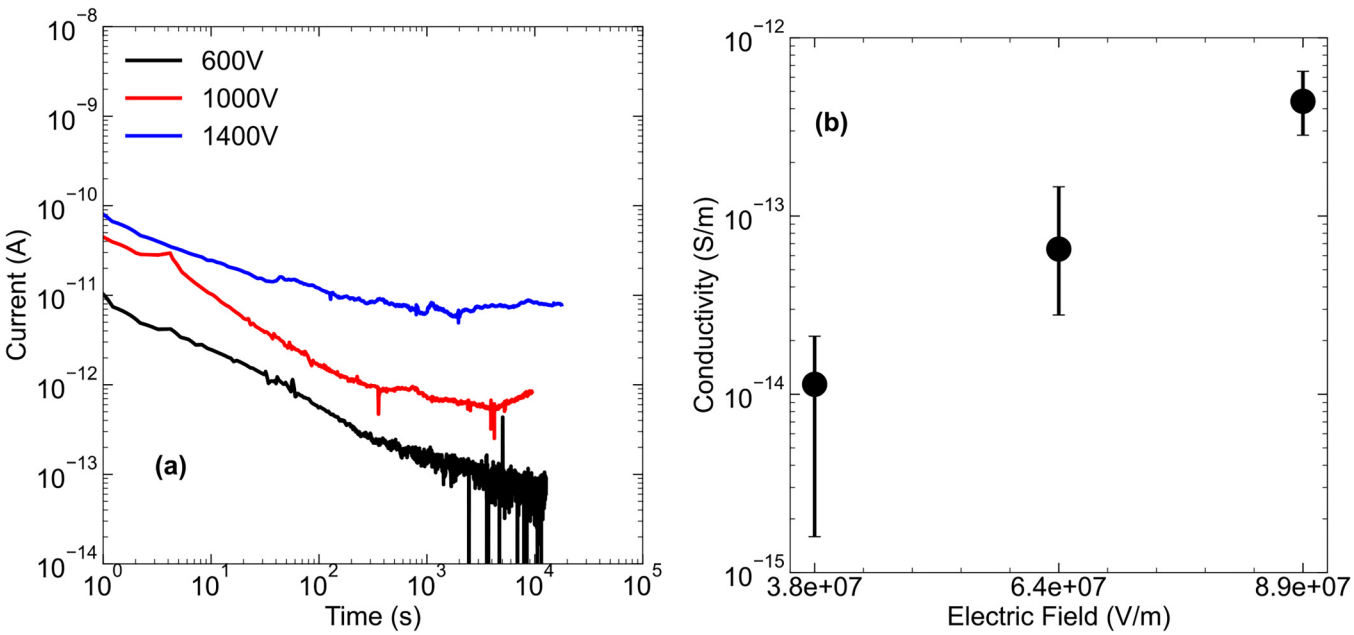

FIG. 2. (a) Transient current of dry samples for different values of the applied voltage V_{DC}. (b) Average value of the steady-state conductivity as a function of the applied electric field. The error bars show the maximum and minimum observed value.

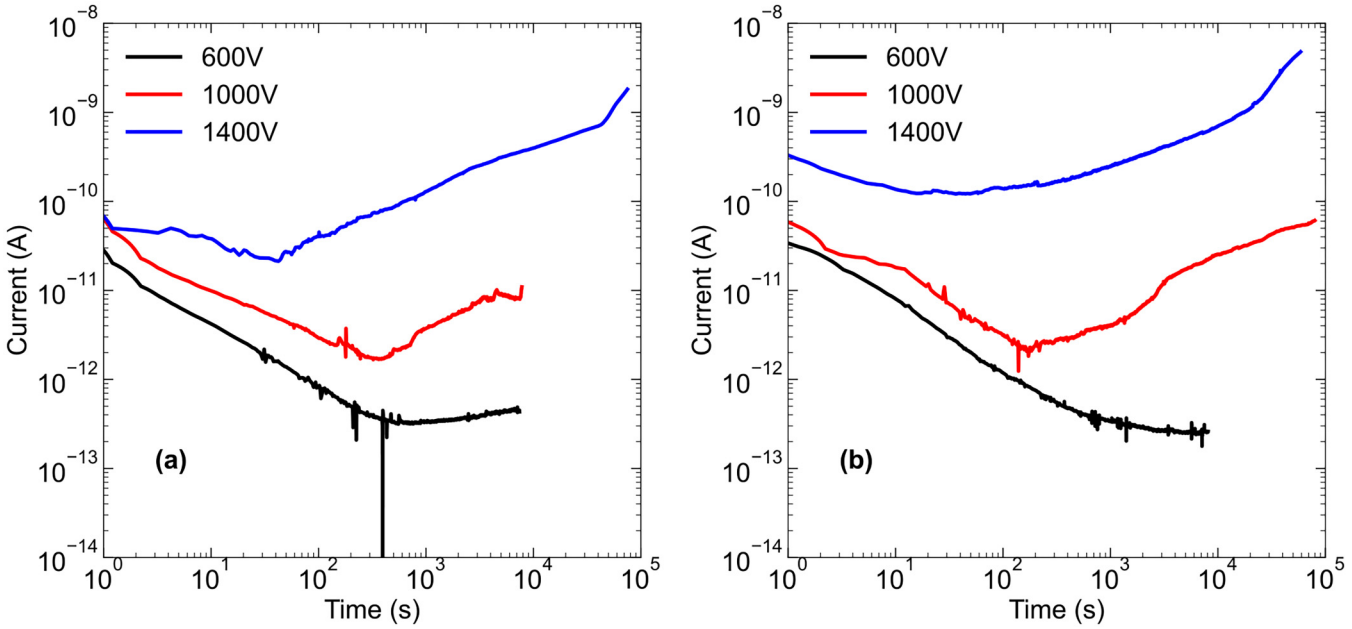

FIG. 3. Transient current of wet samples for different values of the applied voltage. Moisture uptake in a climatic chamber at 85 °C/85% RH for (a) 96 and (b) 168 h.

III. NUMERICAL SIMULATIONS

In order to provide a physical explanation of the experimentally observed phenomena, numerical simulations have been performed by adopting a bipolar transport model accounting for equations of free and trapped electrons and holes as a starting point.[14,15] After a brief review of the adopted bipolar model, the role of humidity on the $i(t)$ curves is clarified through the additional transport equations of positive and negative ions, leading to the comprehensive prediction of the experimental features.

A. Simulation setup and a transport model

The structure under study is characterized by a complex 2D geometry [Fig. 1(b)]. A preliminary analysis has been carried out to identify 2D effects at the corners. Despite a slight increase of the electric field expected at the corners of the interdigitated capacitor, its overall impact on conductivity measurements remains negligible provided that the applied field stays well below the measured breakdown voltage, which, under DC conditions, is around 3000 V.[16] This occurs because the portion of the electrode area influenced by corner effects is indeed minimal compared to the region where the contacts exhibit a well-defined parallel-plate structure. Thus, the interdigitated capacitor in Fig. 1 can be approximated as a one-dimensional parallel-plate capacitor to significantly reduce computational costs. The simulation domain has been discretized using a non-uniform mesh, with refinements near the metal/EMC interfaces to mitigate converge issues. According to Refs. 8, 14, and 15, the carrier dynamics of dry EMCs are simulated by using the bipolar charge-transport model, which consists of four continuity equations that describe the behavior of free electrons (n), free holes (p), trapped electrons (n_t), and trapped holes (p_t). The continuity equations are coupled with Poisson's equation to accurately determine the electrostatic potential within the system. The full set of equations is reported in the Appendix. Carrier mobilities are treated as field-dependent, following the hopping model. Diffusivity is related to mobility through the Einstein relation. Mobility has been set to zero for trapped charges. The trapping and recombination mechanisms accounted for in the bipolar charge-transport model typically include electron/hole capture and emission from traps, trap-assisted recombination, and direct band-to-band recombination. All mechanisms have been consistently implemented in our simulation framework. However, band-to-band recombination is generally considered negligible in epoxy resins due to their amorphous nature and the dominance of localized trap states. Experimental studies on diglycidyl resin ether of bisphenol-A (DGEBA) showed that electroluminescence and recombination-induced luminescence originate from traps, rather than from delocalized band states, indicating that charge recombination proceeds primarily through trap-mediated mechanisms.[17] As a result, the corresponding recombination term has been included in the model for completeness but is set to zero in all simulations presented in this work. Schottky boundary conditions have been applied for free carriers, assuming no extraction barrier, while no-flux conditions have been imposed on trapped carriers. To improve the numerical convergence and reduce computational cost, a small uniform density is set as an initial condition for both free and trapped charges. Such values are low enough not to influence the resulting current transients $i(t)$. To simulate the effects of

moisture in wet samples, two additional continuity equations have been introduced for positive and negative ions, with no source terms and zero-flux boundary conditions. It is assumed that the ion mobilities in dry samples are so low that their contribution to the accumulation of hetero-charges close to the electrodes is negligible. This is consistent with the space-charge measurements carried out on thicker samples in dry conditions.[8] Simulations have been performed in the COMSOL Multiphysics® framework, by using the transport of a diluted species module to solve continuity and transport equations for each kind of carrier together with the Poisson equation module coupling all the different carrier equations to the Poisson one. A detailed description of the model is provided in the Appendix along with the parameter sets. As far as the model is concerned, parameters for both positive and negative charge carriers are required to properly simulate the charge-transport properties of the material. However, from the conductivity measurements as performed in this work, it is not possible to extract their separate contribution to the total current and to the amount of an accumulated space charge. In the EMC material under study, however, the influence of positive/negative charges at the electrodes is quite similar with only slight changes in the net charge density with time, as observed from pulsed electro-acoustic (PEA) measurements performed on thick EMC samples.[8] Due to the limited resolution of the PEA technique, it is not possible to directly measure the space-charge dynamics in samples with thicknesses of the order of 15 μm. As far as the energetic trap distribution is concerned, the implementation of the isothermal surface potential decay (ISPD) method was proposed in the literature. Unfortunately, fabricating flat and very thin films of this material as required for this technique is challenging when compared with other polymers due to the large fraction of micrometer-sized silica fillers (70%–90%) leading to high surface roughnesses. Thus, since the aim is to be directly comparable with available experimental $i(t)$ data, conduction and trap parameters for electrons and holes are set identical by default.[14] The same approach is adopted for positive and negative ions. All the parameters used to perform the simulations reported in Subsection III B are explained in the Appendix, and the corresponding values are listed in Table I.

B. Effects of traps and humidity on the transient current

In order to get physical insight in the current dynamics of the EMC structure under investigation, it is useful to decompose the problem by separating the contribution of free carriers, traps, and, eventually, ions.

The simplest transport configuration is the one in which only free electrons and holes are accounted for, with source terms set to zero. Therefore, the system of equations to be solved reduces to only two continuity equations, coupled to the Poisson equation (set 1 in Table I). As reported in Fig. 4(a), when the capacitor is subjected to the step-voltage stress, three different regions can be distinguished in the $i(t)$ curves. The corresponding time evolution of the space charge is reported in the contour plot of Fig. 4(b). After the voltage step is applied, a current reduction is observed due to homo-charge formation close to the electrodes [region (i)]. Positive and negative injected charges move toward the center of the sample, and after a few tens of seconds, their distributions begin to overlap leading to a reduction of the net space charge. This induces the increase of the electric field close to the electrodes enhancing the charge injection due to the Schottky-barrier reduction. For this reason, a current increase can be observed, corresponding to region (ii). This mechanism persists until the net space charge in the sample becomes zero and the system approaches the steady state [region (iii)].

When trapping effects are included, two additional continuity equations need to be solved.[15] Two symmetric trap levels are assumed. The first one, with energy depth referred to the valence band, is responsible for the trapped holes p_t. Such traps are neutral when unoccupied, while carry the positive charge of one hole when filled. The second one, at the same energy depth from the conduction band, is responsible for trapped electrons n_t. It is neutral when unoccupied, while carries the negative charge of one electron when filled. They both are coupled with the free carrier equations through trapping and de-trapping coefficients in the source term (s_n, s_p) in the continuity equations.[14] Parameters used for these simulations have been reported in set 2 of Table I. The charge trapping significantly affects $i(t)$ in region (ii) suppressing the current increase observed in the previous case. Under such assumption, the $i(t)$ curve as reported in Fig. 5(a) shows a limited current in steady state as usually observed in experiments during the charging phase of insulators. It can be observed that current reduces with time due to homo-charge formation as before in region (i). However, as shown by the corresponding 2D contour plot reported in Fig. 5(b), there is a significant amount of space charge in the sample bulk even in a steady state, supporting a reduced electric field at the electrodes. In order to achieve such a space-charge configuration, it is fundamental to account for trap-assisted recombination. Without the latter mechanism, at some point in time, all traps will become filled, preventing further trapping events. As a result, the material would behave like a trap-free insulator, leading to a corresponding increase of the current, as observed in the previous case. This is shown in Fig. 6(a), where $i(t)$ without trap-assisted recombination for both charge carriers (S_1 and S_2 are set equal to zero) is compared with the case where this phenomenon is included and the trap-free condition. Moreover, in Fig. 6(b), the corresponding electron average trapping rate $c_n n(1 - n_t/N_T)$ is shown: when trap-assisted recombination is neglected, the total trapping rate decreases to zero as the traps become completely filled. On the contrary, when trap-assisted recombination is accounted for, strong trapping persists even under steady-state conditions.

The current reduction with time is, thus, due to the interplay between trapping of electrons from the conduction band and their recombination with trapped holes. Upon the application of a step-voltage stress, a small fraction of the holes injected from the anode (a positively charged electrode) are trapped, giving rise to a high p_t close to the electrode. Concurrently, electrons injected from the cathode move across the sample and recombine with trapped holes as soon as they encounter them. Since the recombination rate is proportional to the product $n \cdot p_t$, it is most pronounced in regions where both n and p_t are significantly large. Due to trap-assisted recombination, the electron concentration gradually decreases from the cathode toward the anode, resulting in a lower n near the latter. A slight increase may occur very close to the anode although

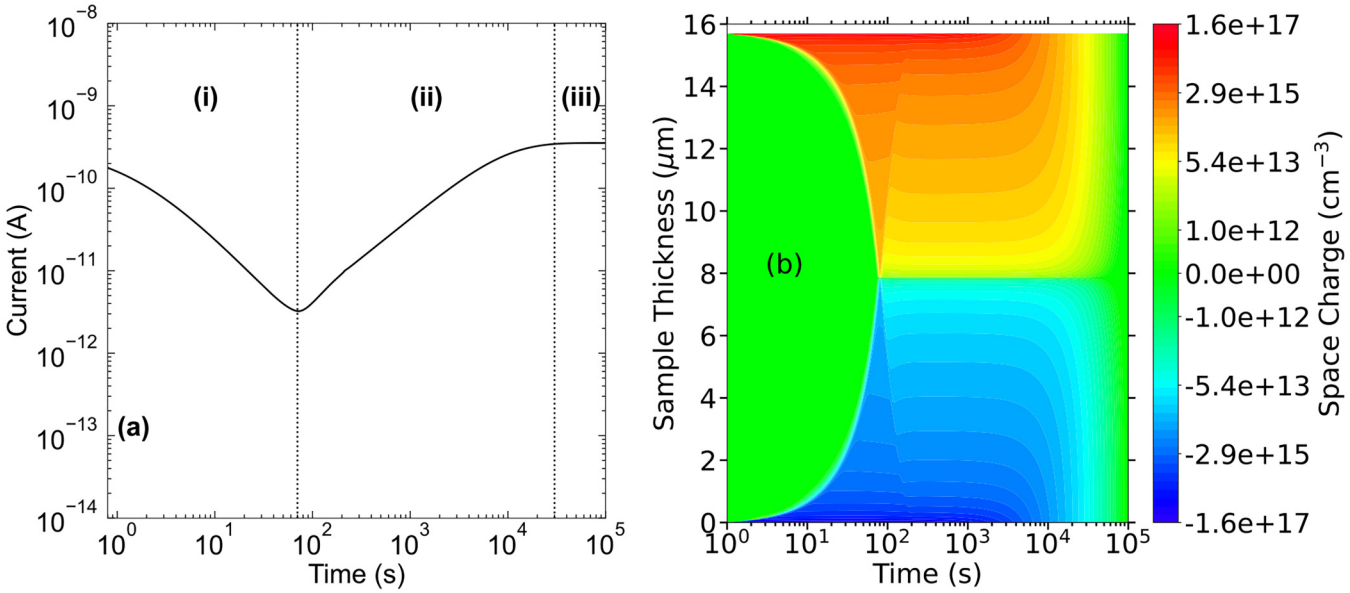

FIG. 4. (a) Simulated transient current with only free electrons and holes in the EMC. A step voltage is applied at t = 0 with $V_{DC} = 1400$ V. (b) Corresponding 2D contour plot of the space-charge time evolution in the 1D capacitor.

remaining negligible compared to the free hole concentration near the anode. As a result, a non-zero space charge persists even under steady-state conditions. Depending on the trap parameters, a partial reduction of the homo-charge may still be present, resulting in a slight increase in current [region (ii) of Fig. 5(a)] before the steady state is reached [region (iii)]. In Fig. 7, the free electron and trapped hole concentrations along the sample are reported for four different stress times. At the beginning, electrons are injected from

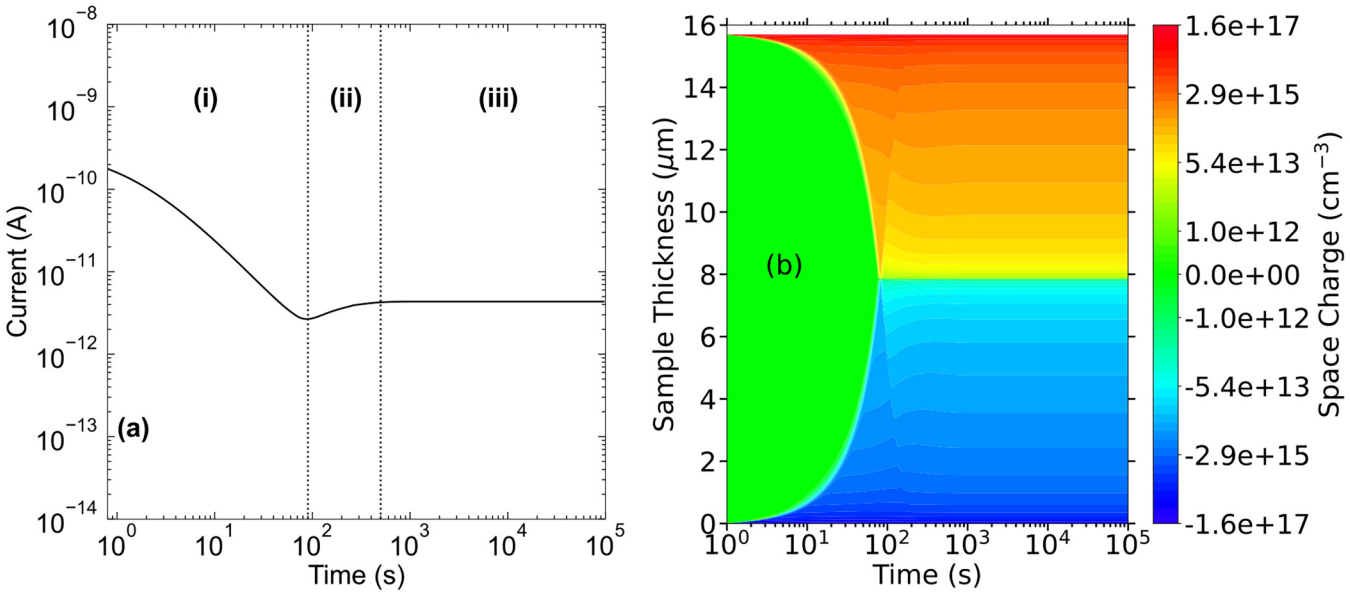

FIG. 5. (a) Simulated transient current with both conduction and trapped electrons and holes in the EMC. A step voltage is applied at t = 0 with $V_{DC} = 1400$ V. (b) Corresponding 2D contour plot of the space-charge time evolution in the 1D capacitor.

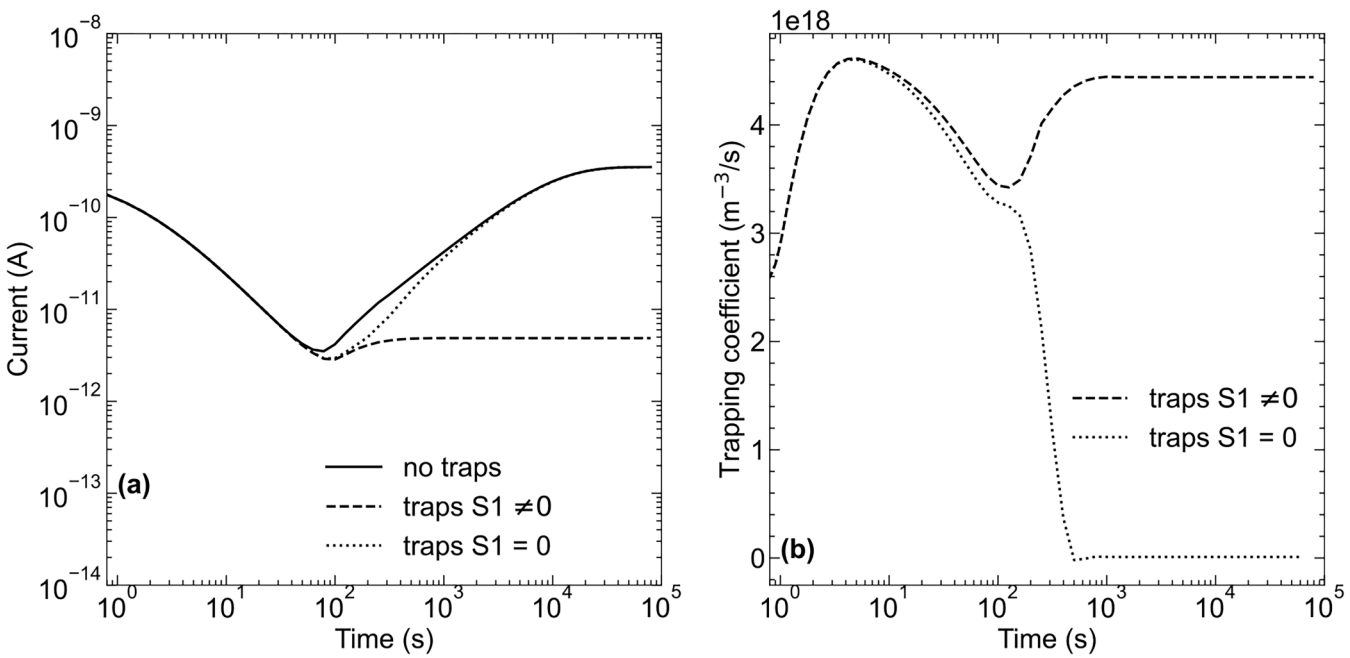

FIG. 6. (a) Simulated transient current with or without trap-assisted recombination compared with the trap-free case. A step voltage is applied at t = 0 with $V_{DC} = 1400$ V. (b) Corresponding average trapping coefficient $c_n n(1 - n_t/N_T)$ as a function of time.

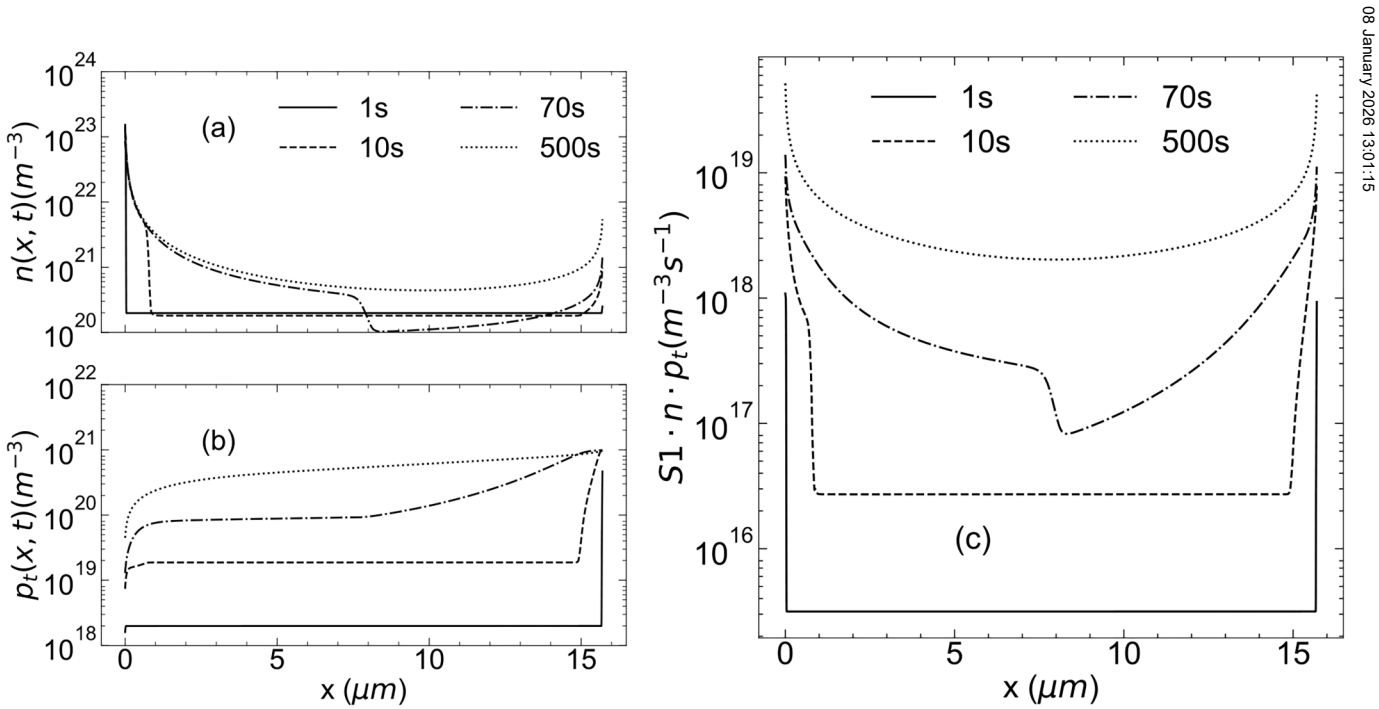

FIG. 7. (a) Free electron concentration n, (b) trapped hole concentration p_t, and (c) trap-assisted recombination rate $S1 \cdot n \cdot p_t$ extracted at four different stress times: beginning of the step voltage (1 s), during the homo-charge formation (10 s), at the onset of the space-charge overlap (70 s), and at the end of the space-charge redistribution (500 s).

the cathode and drift toward the anode under the influence of the electric field, resulting in a higher electron concentration near the cathode. In contrast, the concentration of trapped holes p_t decreases from anode to cathode. This behavior arises because p_t is strongly dependent on the local free hole concentration, which is higher near the anode where hole injection occurs. At approximately t = 70 s, the region with high p_t covers mostly the full distance from anode to cathode and overlaps with the region where n is significantly high. This leads to a significant reduction of the free electrons caused by the strong recombination as confirmed by the term ($S1 \cdot n \cdot p_t$) reported in Fig. 7(c).

When exposed to an environment with high relative humidity, water molecules diffuse into the EMC (Fick absorption) and reach the quasi-saturation of the gravimetric curves after about 48 h in thick samples.[12] The second non-Fickian stage of water uptake is ascribed to specific reactions with the resin,[18] leading to chemical modifications in the material structure that significantly modify the transport properties.[19] In order to account for the presence of positive and negative ions, two additional continuity equations are needed. To simplify the model as much as possible, and reduce the number of fitting parameters, all source terms have been set to zero for ions. In addition, in order to highlight their role in the $i(t)$ curves, the free electron and hole equations are accounted for with source terms set to zero as well (set 3 in Table I). It will become clear later that this approach is the most efficient one in the description of the current dynamics of wet EMC samples under high biases. In Fig. 8(a), the current dynamics of the simulation that includes free positive and negative ions is reported and compared with the previously discussed case in which only free electrons and holes have been accounted for. The corresponding 2D contour plot of the space-charge time evolution is reported in Fig. 8(b). In the $i(t)$ curves, the same behavior can be observed for low stress times, while a clear deviation is visible at $t \approx 3000$ s due to accumulation of ions close to the contacts. At $t \approx 40\,000\,s$, a sharp increase in the current is observed, which is attributed to enhanced charge injection from the electrodes. This results from a locally intensified electric field at the electrodes, caused by hetero-charge accumulation due to ion migration. This is clearly visible in the space-charge contour plot, where strong hetero-charge formation is observed at large stress times. The curve with mobile ions is in nice qualitative agreement with experiments on wet samples at large biases (Fig. 3).

Finally, to demonstrate that the simultaneous presence of a large trap concentration and ions is not compatible with the experimental observations at large biases, we performed simulations, including trapping phenomena in the electron and hole equations and free mobile ions without source terms as in the previous case (set 4 in Table I). The resulting transient current is shown in Fig. 9(a), where it is compared with the case of Fig. 8 with ions. It deviates significantly from the experimental data, as it exhibits a prolonged low-current plateau for 300 s $< t <$ 3000 s, which is not observed in the measurements. This discrepancy arises because charge trapping and trap-assisted recombination still dominate in the current dynamics. A limited increase is experienced in region (III) due to the ionic transport and consequent ionic accumulation, but their role is significantly suppressed. As illustrated in Fig. 9(b), the corresponding space-charge distribution reveals a reduction of the total homo-charge but no significant hetero-charge formation up to $t = 10^5$ s, as the accumulated ion density remains too low to counterbalance the pre-existing space charge. Thus, the

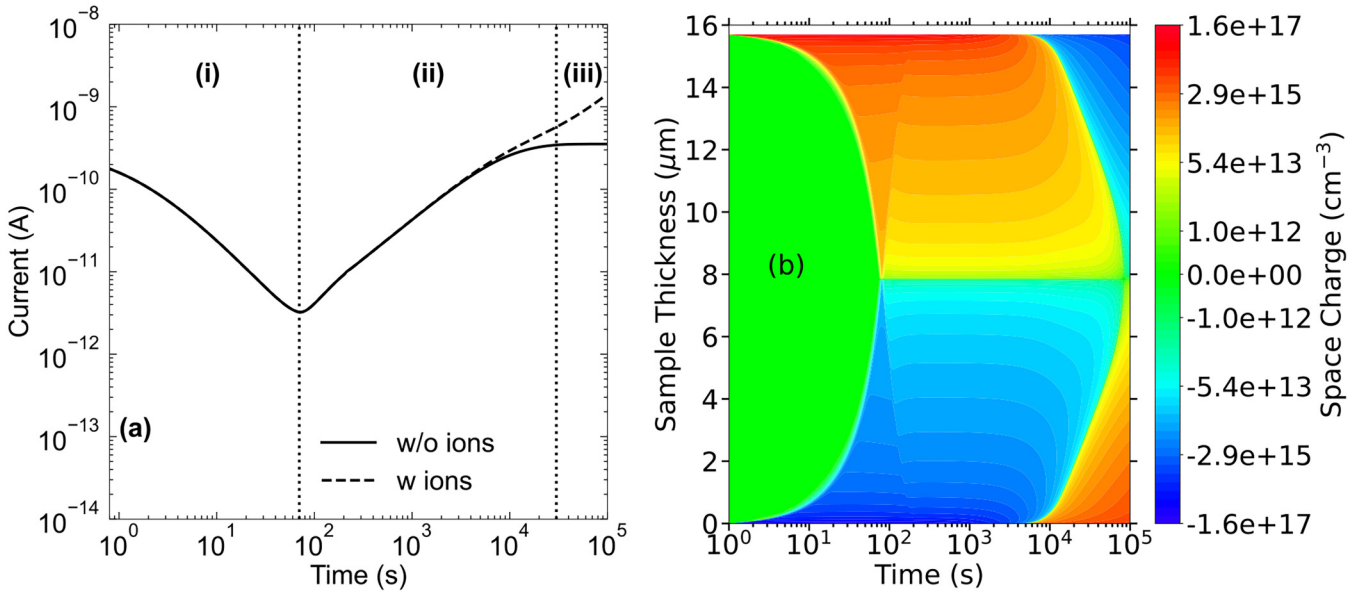

FIG. 8. (a) Simulated transient current with free electrons/holes and positive/negative ions in the EMC. A step voltage is applied at t = 0 with $V_{DC} = 1400$ V. (b) Corresponding 2D contour plot of the space-charge time evolution in the 1D capacitor.

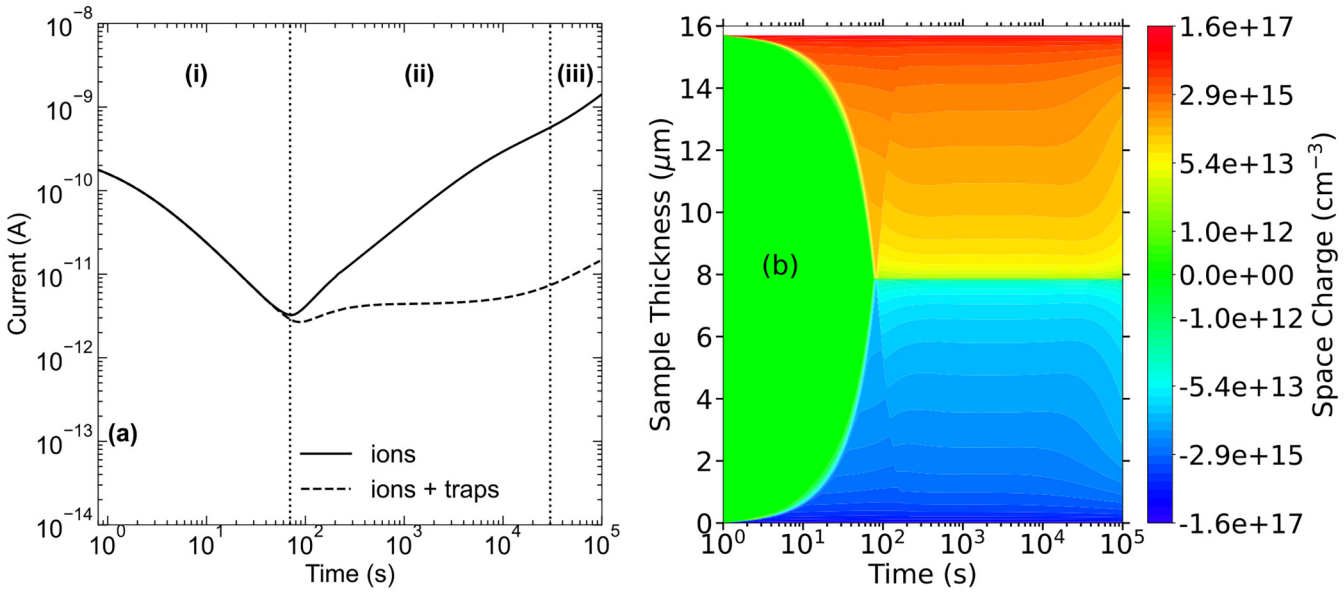

FIG. 9. (a) Simulated transient curve where both ions and trapping effects are accounted for compared with the case in which only ions are present. A step voltage is applied at t = 0 with $V_{DC} = 1400$ V. (b) Corresponding 2D contour plot of the space-charge time evolution in the 1D capacitor in the case when both traps and ions are present.

experimentally observed increase of current in wet samples can be attributed to limited/negligible trapping effects, which prevent recombination phenomena and lead to a reduction of the net space charge due to the presence of large n and p concentrations in the same region of the device. This is essential to reproduce the experimentally observed double slope in the $i(t)$ curves, as it facilitates hetero-charge accumulation.

As a result, the device does not reach a steady-state regime, and a second sharp increase of the current for large voltages and stress times arises from hetero-charge formation due to the presence of ions.

IV. DISCUSSION

The proposed model is used to fit all the available experimental measurements reported in Subsection II B. This final model validation was done in three steps, leading to the coherent description of the main features in any stress condition. The corresponding parameters set are listed in Table II at the end of the Appendix. The $i(t)$ curves of dry EMC samples [Fig. 10(a)] show a current decrease with time followed by the steady state: it can, thus, be reproduced by assuming the presence of traps and field-dependent mobility. The discrepancies between simulations and experiments are similar to those observed in previous works[20] and can be related to a simplified treatment of the trapping phenomena, which are accounted for by assuming the presence of two symmetric trap levels. Thus, the dispersive nature of transport, which is typically associated with a broad distribution of capture and release times for charge carriers, leading to non-exponential relaxation dynamics, cannot be accurately reproduced.[21]

In Figs. 10(b) and 10(c), simulations and experiments of wet samples are compared. The main features of the transient current characteristics are nicely reproduced confirming the validity of the proposed modeling approach. Under low biases, wet samples do not show significant differences in the I(t) curves when compared with the corresponding dry measurements, suggesting that the impact of moisture is very limited. Consequently, it has been assumed that at 600 V, the role of ions is negligible by fixing their mobility to zero. To account for the slight increase in the steady-state current in the wet cases, reduced capture coefficients c_n and c_p have been used. In order to reproduce the current dynamics of wet samples at high electric fields ($V_{DC} \geq 1000$ V), it has been assumed that traps play a very limited role, reflected in a further reduction of the capture coefficient, as expected from the observed current increases. According to experimental observations of the $i(t)$ curves, sufficiently large ionic mobility has been used at 1400 V for the 96 h case and at both 1000 and 1400 V for the 168 h case. By doing so, it is possible to allow a significant accumulation of hetero-charge and give rise to the observed sharp increase of the current at large stress times. Different water uptakes have been, thus, modeled by reducing the capture coefficient and increasing the ionic concentrations with the preconditioning time. The assumptions adopted in the wet case are in agreement with previous works in the literature. From an experimental point of view, Ahn *et al.*[8] showed through PEA measurements that wet samples exhibit a reduction of homo-charge with time together with an increase of hetero-charge. As shown in Fig. 11, where the simulated space-charge profile for the 168 h case at 1000 V is reported, a similar trend has been found in this work, thereby strengthening

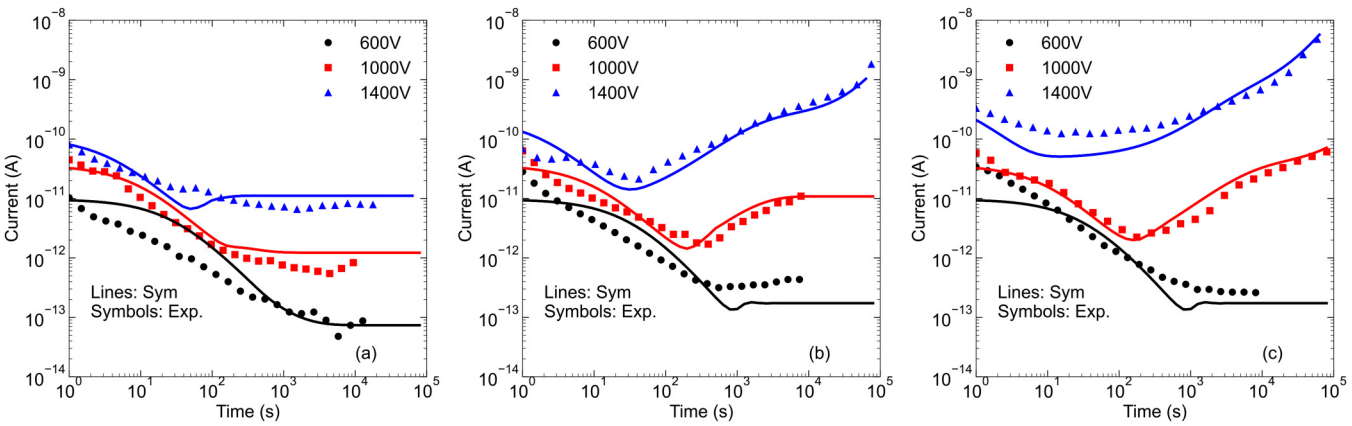

FIG. 10. Measured currents as a function of time for different values of stress voltages compared with simulations. (a) Dry samples, (b) wet samples with 96 h of preconditioning, and (c) wet samples with 168 h of preconditioning.

the validity of this approach. The reduction of homo-charge can be emulated by assuming that, when trapping effects are limited or even absent, electron and hole profiles overlap and give a net reduction of space charge. Conversely, the increase in the hetero-charge is ascribed to the presence of ions: Suzuki *et al.*[19] demonstrated through molecular-dynamics simulations that, under wet conditions, Cl^- ions become surrounded by water molecules, which lower the hopping potential barrier, thereby increasing their mobility. Such an effect is strongly enhanced by the presence of high electric fields, thereby clarifying why the $i(t)$ curves remain almost unaffected by the presence of moisture at low biases.

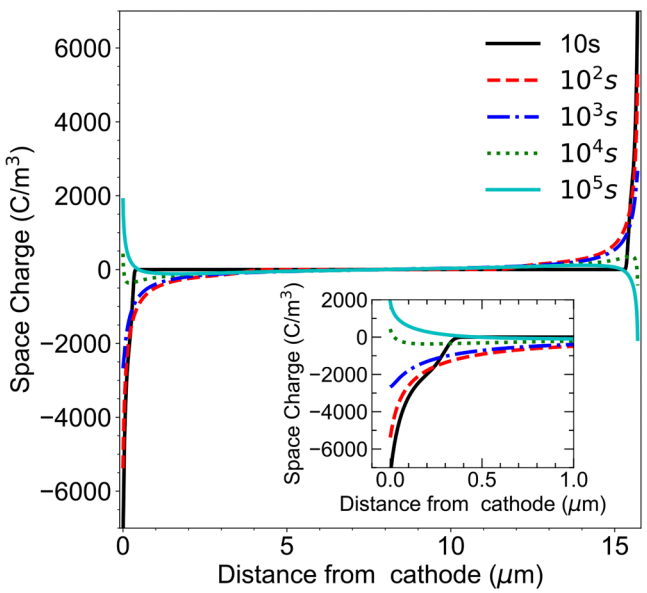

FIG. 11. Simulated space charge in the EMC sample for the 168 h case at 1000 V. The inset shows a magnified version of the space-charge profile close to the cathode.

V. CONCLUSION

In this study, a detailed investigation of the behavior of epoxy-based molding compounds (EMCs) under DC step stress has been provided with particular emphasis on the role played by moisture. By combining experimental measurements with numerical simulations, it has been demonstrated that the presence of water significantly affects the electrical characteristics of EMCs, primarily by limiting trapping effects and facilitating the formation of hetero-charge due to water dissociation. Wet samples exhibit a unique current increase over time at high voltages, attributed to the enhanced ion mobility. Ions migrate toward the electrodes and enhance hetero-charge accumulation. This phenomenon prevents the system from reaching a steady-state current regime and poses challenges for the long-term reliability of EMCs in high-moisture environments. The results presented here clarify the role of humidity on the EMC electrical properties and offer valuable insights for improving the design and reliability of HV-IC packages used in harsh environmental conditions, emphasizing the need for limiting moisture effects in future material and device designs.

AUTHOR DECLARATIONS

Conflict of Interest

The authors have no conflicts to disclose.

Author Contributions

Luigi Balestra: Conceptualization (lead); Data curation (lead); Formal analysis (lead); Investigation (lead); Methodology (lead); Writing – original draft (lead). **Mattia Rossetti:** Conceptualization (supporting); Data curation (supporting); Formal analysis (supporting); Funding acquisition (equal); Investigation (supporting); Methodology (supporting); Supervision (equal); Validation (equal);

Writing – review & editing (equal). **Elena Gnani:** Funding acquisition (equal); Project administration (equal); Supervision (equal); Writing – review & editing (equal). **Susanna Reggiani:** Conceptualization (supporting); Data curation (supporting); Formal analysis (supporting); Funding acquisition (lead); Investigation (supporting); Methodology (supporting); Project administration (lead); Supervision (lead); Writing – review & editing (lead).

DATA AVAILABILITY

The data that support the findings of this study are available within the article.

APPENDIX: BIPOLAR CHARGE-TRANSPORT MODEL

In order to properly describe charge-transport phenomena in the EMC, the Poisson equation is solved consistently with six continuity equations, one for each species.

Poisson's equation reads

$$\nabla \cdot (\varepsilon_0 \varepsilon_r \vec{E}) = q(p - n + p_t - n_t + i^+ - i^-), \tag{A1}$$

where $\vec{E}$ is the electric field, ε_0 is the vacuum permittivity, ε_r is the relative permittivity of the material, and q is the elementary charge. The total charge density is given by the contribution of free electrons n, free holes p, trapped electrons n_t, and trapped holes p_t. Moreover, for wet samples, positive and negative ions are accounted for. They are indicated as i^+ and i^-, respectively. The charge carrier dynamics is described by the following continuity equations:

$$\frac{\partial n}{\partial t} + \nabla \cdot (-n\mu_n \vec{E} - D_n \nabla n) = s_n, \tag{A2}$$

$$\frac{\partial p}{\partial t} + \nabla \cdot (p\mu_p \vec{E} - D_p \nabla p) = s_p, \tag{A3}$$

$$\frac{\partial n_t}{\partial t} = s_{n_t}, \quad \frac{\partial p_t}{\partial t} = s_{p_t}, \tag{A4}$$

$$\frac{\partial i^+}{\partial t} + \nabla \cdot \left(i^+ \mu_{ion} \vec{E} - D_{ion} \nabla i^+\right) = 0, \tag{A5}$$

$$\frac{\partial i^-}{\partial t} + \nabla \cdot \left(-i^- \mu_{ion} \vec{E} - D_{ion} \nabla i^-\right) = 0, \tag{A6}$$

where $\mu_{n,p,ion}$ is the mobility and $D_{n,p,ion}$ is the diffusion coefficient. In order to account for the mobility field dependence of mobile electrons and holes, the variable range hopping model (VRH) has been used. It can be expressed as

$$\mu_{n,p} = \frac{2\lambda\nu}{|\vec{E}|} \exp\left(\frac{-qw_c}{k_B T}\right) \sinh\left(\frac{q\lambda|\vec{E}|}{2k_B T}\right), \tag{A7}$$

where λ is the hopping distance , ν is the attempt to escape the frequency, w_c is the hopping barrier height for electrons and holes, k_B is the Boltzmann constant, and T is the temperature. The same values of λ and w_c have been used for both free electrons and holes. A constant mobility model has been employed for both positive and negative ions, using the same mobility parameter μ_{ion}, implying identical transport properties for both species. Mobilities and diffusion coefficients are uniquely related through the Einstein relations. The source term s accounts for trapping mechanisms; source terms account for trapping and de-trapping phenomena and trap-assisted and band-to-band recombination. Source terms can be written as

$$s_n = -c_n n\left(1 - \frac{n_t}{N_T}\right) + e_n n_t - qS_1 np_t - qS_3 np, \tag{A8}$$

$$s_{n_t} = c_n n\left(1 - \frac{n_t}{N_T}\right) - e_n n_t - qS_2 n_t p, \tag{A9}$$

$$s_p = -c_p p\left(1 - \frac{p_t}{P_T}\right) + e_p p_t - qS_2 pn_t - qS_3 np, \tag{A10}$$

$$s_{p_t} = c_p p\left(1 - \frac{p_t}{P_T}\right) - e_p p_t - qS_1 p_t n. \tag{A11}$$

In the above equations, c_n and c_p are the capture coefficients for electrons and holes, respectively, while e_n and e_p are the corresponding emission coefficients. The latter are usually expressed in terms of a trap depth $E_{t_{n,p}}$ and attempt-to-escape frequency $\nu = k_B T/h$ as

$$e_{n,p} = \nu \exp\left(-\frac{E_{t_{n,p}}}{k_B T}\right), \tag{A12}$$

where N_T and P_T denote the maximum concentration of available trap states for electrons and holes, respectively.

S_1 accounts for trap-assisted recombination between free electrons and trapped holes, S_2 corresponds to recombination between free holes and trapped electrons, and S_3 describes direct band-to-band recombination between free electrons and holes.

A Schottky boundary condition has been assumed for injected carriers, while no extraction barrier has been accounted for at the electrodes. For electrons, the flux injected at the cathode is

$$J_{n,c} = AT^2 \exp\left(-\frac{\Phi_{B,e}}{k_B T}\right) \exp\left(\frac{q}{k_B T}\sqrt{\frac{qE}{4\pi\varepsilon_0\varepsilon_r}}\right), \tag{A13}$$

where A is the Richardson constant and $\Phi_{B,e}$ is the injection barrier for electrons. The flux extracted at the anode is

$$J_{n,a} = -n\mu_n \vec{E} - D_n \nabla n. \tag{A14}$$

Analog equations can be written for holes by defining a hole Schottky barrier $\Phi_{B,p}$.

For traps and ions, the boundary condition is

$$J = 0. \tag{A15}$$

The total external current at the electrodes is given by

$$J_{tot} = J_n + J_p + \varepsilon_0 \varepsilon_r \frac{\partial E}{\partial t}. \tag{A16}$$

All the parameter sets used in this work are reported in Tables I and II.

TABLE I. List of parameters used for simulations reported in Sec. III B.

Parameter name	Symbol	Set 1	Set 2	Set 3	Set 4	Unit
Traps	…	No	Yes	No	Yes	…
Ions	…	No	No	Yes	Yes	…
Corresponding figures		4	5–7	8	9	
DC bias	V_{DC}	1400	1400	1400	1400	V
Relative dielectric constant	ε_r	3.9	3.9	3.9	3.9	…
Initial free charge concentration	n_0, p_0	2×10^{20}	2×10^{20}	2×10^{20}	2×10^{20}	m^{-3}
Boundary conditions						
Schottky barrier	$\Phi_{B,e}$, $\Phi_{B,p}$	1.02	1.02	1.02	1.02	eV
Mobility						
Hopping distance	λ	2.1×10^{-9}	2.1×10^{-9}	2.1×10^{-9}	2.1×10^{-9}	m^{-1}
Hopping barrier	w_c	0.80	0.80	0.80	0.80	eV
Traps						
Initial trapped-charge concentration	$n_{t,0}$, $p_{t,0}$	…	2×10^{18}	…	2×10^{18}	m^{-3}
Trap concentration	N_t, P_t	…	1×10^{21}	…	1×10^{21}	m^{-3}
Capture coefficient	c_n, c_p	…	0.01	…	0.01	s^{-1}
Trap depth	$E_{t_{n,p}}$, $E_{t_{n,p}}$	…	1.05	…	1.05	eV
Electron trap-assisted recombination	S_1	…	5×10^{-5}	…	5×10^{-5}	$m^3C^{-1}s^{-1}$
Hole trap-assisted recombination	S_2	…	5×10^{-5}	…	5×10^{-5}	$m^3C^{-1}s^{-1}$
Band-to-band recombination	S_3	0	0	0	0	$m^3C^{-1}s^{-1}$
Ions						
Ions concentration	i^+, i^-	…	…	1×10^{22}	1×10^{22}	m^{-3}
Ions mobility	μ_{ion}	…	…	1×10^{-19}	1×10^{-19}	$m^2V^{-1}s^{-1}$

TABLE II. List of parameters used for simulations reported in Fig. 10. If, for a given parameter, a list of three different values is provided, it means that different values were used for each simulated bias (600, 1000, and 1400 V).

Parameter name	Symbol	Dry	Wet 96 h	Wet 168 h	Unit
Relative dielectric constant	ε_r	3.9	3.9	3.9	…
Initial free charge concentration	n_0, p_0	2×10^{20}	2×10^{20}	2×10^{20}	m^{-3}
Boundary conditions					
Schottky barrier	$\Phi_{B,e}$, $\Phi_{B,p}$	1.05	1.03	1.03	eV
Mobility					
Hopping distance	λ	3×10^{-9}	3×10^{-9}	3×10^{-9}	m^{-1}
Hopping barrier	w_c	0.795	0.795	0.795	eV
Traps					
Initial trapped-charge concentration	$n_{t,0}$, $p_{t,0}$	2×10^{18}	2×10^{18}	2×10^{18}	m^{-3}
Trap concentration	N_t, P_t	1.75×10^{21}	1.75×10^{21}	1.75×10^{21}	m^{-3}
Capture coefficient	c_n, c_p	5×10^{-3}	5×10^{-4}, 3×10^{-4}, 0	5×10^{-4}, 5×10^{-5}, 0	s^{-1}
Trap depth	$E_{t_{n,p}}$, $E_{t_{n,p}}$	1.05	1.05	1.05	eV
Electron trap-assisted recombination	S_1	5×10^{-5}	5×10^{-5}	5×10^{-5}	$m^3C^{-1}s^{-1}$
Hole trap-assisted recombination	S_2	5×10^{-5}	5×10^{-5}	5×10^{-5}	$m^3C^{-1}s^{-1}$
Band-to-band recombination	S_3	0	0	0	$m^3C^{-1}s^{-1}$
Ions					
Ions concentration	i^+, i^-	…	1×10^{22}	2×10^{22}	m^{-3}
Ions mobility	μ_{ion}	…	0, 0, 1×10^{-19}	0, 2×10^{-20}, 1×10^{-19}	$m^2V^{-1}s^{-1}$

REFERENCES

[1]R. Wazalwar, M. Sahu, and A. M. Raichur, Nanoscale Adv. **3**, 2741 (2021).
[2]J. Sidhu, G. Lathkar, and S. Sharma, J. Inst. Eng. India Ser. C **100**, 283 (2019).
[3]Y. Wang, Y. Ding, and Y. Yin, Energies **15**, 6670 (2022).
[4]L. Balestra, E. Gnani, M. Rossetti, R. Depetro, and S. Reggiani, IEEE Trans. Electron Devices **71**(4), 2565–2569 (2024).
[5]L. Balestra, E. Gnani, S. Reggiani, M. Rossetti, and R. Depetro, in *2024 IEEE Latin American Electron Devices Conference (LAEDC)* (IEEE, 2024), pp. 1–4.
[6]V. Mathew, E. Wikramanayake, and S. F. Chopin, in *2020 IEEE 70th Electronic Components and Technology Conference (ECTC)* (IEEE, 2020), pp. 504–511.
[7]M. D. Placette, X. Fan, J.-H. Zhao, and D. Edwards, Microelectron. Reliab. **52**, 1401 (2012).
[8]W. Ahn, M. A. Alam, D. Cornigli, S. Reggiani, D. Varghese, and S. Krishnan, IEEE Trans. Dielectr. Electr. Insul. **28**, 2043 (2021).
[9]M. Mamun, A. Mavinkurve, M. van Soestbergen, G. Terzariol, and M. A. Alam, J. Appl. Phys. **135**, 165105 (2024).
[10]L. Balestra, L. Cirioni, A. Cavallini, S. Reggiani, M. Rossetti, M. Gallo, S. Guarnera, and R. Depetro, Solid State Electron. **208**, 108728 (2023).
[11]S. Reggiani, L. Balestra, E. Gnani, M. Rossetti, and R. Depetro, in *2024 8th IEEE Electron Devices Technology & Manufacturing Conference (EDTM)* (IEEE, 2024), pp. 1–3.
[12]D. Cornigli, S. Reggiani, A. Gnudi, E. Gnani, G. Baccarani, D. Fabiani, D. Varghese, E. Tuncer, S. Krishnan, and L. Nguyen, Microelectron. Reliab. **88-90**, 752 (2018).
[13]S. Baranovski, *Charge Transport in Disordered Solids with Applications in Electronics* (John Wiley & Sons, 2006).
[14]S. Le Roy, P. Segur, G. Teyssedre, and C. Laurent, J. Phys. D: Appl. Phys. **37**, 298 (2004).
[15]S. Le Roy and M. Hoang, J. Phys. D: Appl. Phys. **55**, 465303 (2022).
[16]L. Balestra, M. T. Riaz, F. Giuliano, A. Cavallini, S. Reggiani, L. Oldani, S. S. Guarnera, M. Rossetti, and R. Depetro, in *2024 IEEE 26th Electronics Packaging Technology Conference (EPTC)* (IEEE, 2024), pp. 690–694.
[17]V. Griseri, L. A. Dissado, J. C. Fothergill, C. Laurent, and G. Teyssedre, J. Phys. D: Appl. Phys. **34**, 2534 (2001).
[18]W. Ahn, D. Cornigli, D. Varghese, L. Nguyen, S. Krishnan, S. Reggiani, and M. A. Alam, IEEE Trans. Compon. Packag. Manuf. Technol. **10**, 1534 (2020).
[19]H. Suzuki, H. Shimakawa, A. Kumada, and M. Sato, IEEE Trans. Dielectr. Electr. Insul. **29**, 170 (2022).
[20]S. Le Roy, G. Teyssedre, C. Laurent, G. Montanari, and F. Palmieri, J. Phys. D: Appl. Phys. **39**, 1427 (2006).
[21]R. T. Sibatov and V. V. Uchaikin, Phys. Usp. **52**, 1019 (2009).